Published paper

Stovin, V., Bennett, P. and Guymer, I. (2013) *Absence of a hydraulic threshold in small-diameter surcharged manholes*. Journal of Hydraulic Engineering, 139 (9). 984 - 994. ISSN 0733-9429
http://dx.doi.org/10.1061/(ASCE)HY.1943-7900.0000758

The Absence of an Hydraulic Threshold in Small-Diameter Surcharged Manholes

Virginia Stovin[1*], Paul Bennett[2] and Ian Guymer[3]

[1*]Corresponding author, Department of Civil and Structural Engineering, The University of Sheffield, Mappin Street, Sheffield, S1 3JD, UK

v.stovin@sheffield.ac.uk

Tel No.: +44 (0) 114 222 5051

Fax No.: +44 (0) 114 222 5700

[2]Former Research Student, Department of Civil and Structural Engineering, The University of Sheffield, Mappin Street, Sheffield, S1 3JD, UK

[3]School of Engineering, University of Warwick, Coventry, CV4 7AL, UK

i.guymer@warwick.ac.uk

Abstract

Previous research into surcharged manholes has highlighted the existence of a threshold surcharge level that separates two distinctly-different hydraulic regimes. Sharp changes in manhole energy loss and solute transport characteristics occur when the surcharge depth passes through the threshold level. With respect to solute transport, two scale-independent Cumulative Residence Time Distributions (CRTDs) have been identified, corresponding to the below-threshold and above-threshold hydraulic regimes. However, previous studies focused on large diameter manholes, in which the manhole diameter (Φ_m) was at least 4.4 times greater than the pipe diameter (Φ_p). This paper utilizes a validated Computational Fluid Dynamics (CFD) modelling approach to explore the hydraulic behaviour and mixing processes in small-diameter surcharged manholes ($1.5 < \Phi_m/\Phi_p < 4.4$). It is shown that the hydraulic threshold does not exist in the small diameter manholes; instead the flow field is characterised by short-circuiting throughout the full range of surcharge depths. Data generated at low surcharge levels suggests that the mixing effects in the below-threshold region are not independent of surcharge level, as had previously been suggested. The absence of the threshold in small-diameter manholes is explained with reference to jet theory. Several previous studies that have characterised mixing and/or energy losses in surcharged manholes are revisited, allowing findings to be generalised across a broader range of manhole configurations, including effects due to benching and change in outlet angle.

Keywords

Computational Fluid Dynamics (CFD), Cumulative Residence Time Distribution (CRTD), dispersion, energy-loss, manhole, mixing, sewer, solute, surcharge

Introduction

Urban drainage systems mainly comprise lengths of pipes conveying flow between nodal structures, including manholes, settling tanks, storage chambers and CSOs. The predominantly dendritic nature of the system lends itself to one-dimensional flow modelling, and most engineering design requirements for either capacity or water quality can be satisfied using such models. However, the sudden expansions from pipes into structures and contractions out of structures create complex three-dimensional flow fields, and the accurate inclusion of their effect requires knowledge of headloss coefficients for capacity calculations and mixing characteristics to describe water quality changes. The flow field that develops within a structure governs both its energy loss and solute transport characteristics. Tracer studies therefore provide an integrated measure of the effects of the complete three-dimensional flow field.

Manholes are used to accommodate pipe junctions, changes in gradient or direction and access for maintenance. Guymer *et al.* (2005) presented results from a laboratory study describing the retention time and longitudinal dispersion of a solute tracer across circular surcharged manhole structures of different diameters. The manhole, of diameter Φ_m, was positioned symmetrically within a length of pipe of diameter Φ_p, in this case 0.088 m. Surcharge (s) was defined as the level of the free surface in the manhole above the pipe soffit. Four different Φ_m values were considered – 800, 600, 485 and 385 mm – corresponding to Φ_m/Φ_p ratios of 9.1, 6.8, 5.5 and 4.4 respectively. Note that the 485 and 385 mm manholes were referred to as 500 and 400 mm in the original paper.

Two different flow and solute transport regimes have been identified for this specific configuration of surcharged manhole, depending upon whether the surcharge level is below or above a critical threshold level ($s' = 0.258\ \Phi_m$). The two different hydraulic regimes were originally termed pre- and post-threshold. However, to avoid confusion when considering time-dependent scenarios, they will henceforth be referred to as below- and above-threshold. At surcharge levels below the threshold, the flow field is dominated by a chaotic and swirling flow which promotes mixing. The incoming jet shows asymmetry in the horizontal plane, with a clear recirculatory return current in the left portion of the manhole. The vertical flow field is characterised by jet dissipation and mixing throughout the flow depth. Solute trace data demonstrates that the below-threshold flow regime is characterised by good mixing, i.e. significant attenuation of the peak concentration. Above the threshold surcharge level, the vertical flow field comprises two separated flow regions. A dead zone forms in the upper part of the manhole, while the majority of the incoming flow passes straight through the manhole, short-circuiting the upper storage volume. The horizontal flow field is almost symmetric, and the vertical flow field is characterised by limited jet dissipation and mixing. This is reflected in solute traces that typically show limited mixing, short-circuiting and reduced levels of peak attenuation compared with the below-threshold case.

One approach to modelling solute transport within complex engineered systems is to consider the system's Residence Time Distribution (RTD). An RTD describes the system's response to an instantaneous upstream injection, and so conceptually can only be derived from a pulse (or instantaneous injection) experiment. However, responses to other injection types – including the Gaussian-like distributions considered above – may be converted to an RTD via numerical manipulation or deconvolution (Levenspiel, 1972). The Cumulative RTD (CRTD) represents the integral of the RTD, which is usually normalised to sum to unity. CRTDs are inherently scalable. Ignoring any effects of longitudinal dispersion and assuming 'plug flow', the nominal retention time, t_n, within a body of fluid may be estimated from the ratio of the storage volume (V) to the flowrate (Q), ($t_n = V/Q$). Danckwerts (1958) suggested that if a model is geometrically similar to the prototype the normalized CRTD ($t_{nz} = tQ/V$) should be identical for model and prototype.

Based primarily on CFD (Computational Fluid Dynamics)-derived CRTDs, Stovin *et al.* (2010) suggested that the solute transport characteristics of the surcharged manhole described above could be modelled by just two normalized CRTDs, one for below- and the other for above-threshold surcharge. Guymer and Stovin (2011) used deconvolution to reanalyse a portion of the laboratory data presented by Guymer *et al.*, (2005), confirming the validity of the two-CRTD model for manhole mixing. It is important to note that the normalised CRTDs are scale-independent, and hence these findings are directly applicable to full-scale systems.

Guymer *et al.* (2005) suggested that the existence of the dual hydraulic regimes could be explained with reference to jet theory. Rajaratnam (1976) has presented detailed theoretical analyses of the mean flow characteristics for several simple configurations of turbulent jets, together with supporting experimental data. For a circular free jet discharging into a large stagnant body of fluid, the radial velocity discontinuity leads to the development of a shear layer. With distance from the point of entry, the shear layer increasingly invades the uniform-velocity jet on its inside and penetrates into the ambient fluid on its outside. Albertson *et al.* (1950) showed that the core velocity is retained for a distance of approximately 6.2 Φ_p, irrespective of pipe velocity, whilst the jet dissipation region on a free jet spreads at a gradient of 1:5 to the longitudinal axis. Where the jet discharges adjacent to a wall, a shear layer develops on the fluid side, whilst a boundary layer develops on the wall side. In such conditions, Rajaratnam and Subramanya (1967) experimentally confirmed that the core velocity is retained for a slightly greater length, between 6.1 to 7.6 Φ_p.

More complex situations of confined jets have also been analysed by Rajaratnam (1976). However, these are limited to the expansion of axi-symmetric circular jets in circular ducts. There is limited previous work investigating jet decay in a confined chamber (or manhole). A full understanding of the flow regime and energy losses in these structures has typically required experimental analysis or three-dimensional CFD modelling. Pedersen and Mark (1990) investigated the energy losses associated with sewer manholes and

Camino *et al.* (2012) studied vertical jets issuing into a rectangular chamber to quantify energy dissipation. Their results confirm that the boundaries of the chamber produce recirculations in the surrounding fluids, reducing the inflow momentum and promoting more rapid jet decay.

Data presented by Guymer *et al.* (2005) suggested that the threshold surcharge levels for the 800, 600, 485 and 385 mm Φ_m manholes were approximately 220, 156, 121 and 90 mm respectively. Regression through the origin gives a general relationship for the threshold surcharge level, s' = 0.258 Φ_m. Guymer *et al.* (2005) proposed that the threshold level was linked to the jet expansion described by Albertson *et al.* (1950). If the surcharge level exceeds $\Phi_m/5$, then the jet dissipation region will not break the surface. This appears to lead to the development of an upper dead zone, characteristic of the above-threshold hydraulic regime. Conversely, if s < $\Phi_m/5$, then the jet dissipation region will break the free surface within the manhole, leading to the chaotic, well-mixed, hydraulic regime associated with below-threshold surcharge levels. The small difference between the observed trend for the threshold level (s' = 0.258 Φ_m) and the 1:5 gradient associated with the boundary of the theoretical jet dissipation region may reflects the fact that the jet core moves vertically upwards away from the manhole base due to the formation of the boundary layer.

In the UK, the publication 'Sewers for Adoption' (WRc, 2006) suggests that regularly-encountered manhole sizings range from 1200 mm on pipes less than 375 mm diameter (Φ_m/Φ_p > 3.2) up to 1800 mm on 750-900 mm pipes (2.00 < Φ_m/Φ_p < 2.40). These Φ_m/Φ_p ratios fall significantly below the minimum considered in previous manhole mixing studies, i.e. Φ_m/Φ_p = 4.4 (Guymer *et al.*, 2005). Research is required to understand the flow, and pollutant mixing, processes associated with these smaller-diameter manholes.

For Φ_p = 88 mm, the theoretically-determined jet core length of 6.2 Φ_p equates to a distance of approximately 550 mm, suggesting that – for the larger manholes studied by Guymer *et al.* – the core velocity would not be present at the outlet. However, manholes with smaller Φ_m/Φ_p ratios would retain the core jet velocity at the exit to the manhole, and might therefore be expected not to develop the chaotic well-mixed flow conditions even at small surcharge levels. The Guymer *et al.* (2005) study suggested that the threshold was evident at all four manhole diameters, although the presence of the threshold, and the occurrence of well-mixed conditions at surcharge levels below the threshold, became less evident as Φ_m/Φ_p reduced, and at higher discharges. The existence of the well-mixed zone at manhole diameters < 6.2 Φ_p is consistent with others' observations that the jet decay is more rapid in confined systems. However, it is expected that decreasing Φ_m/Φ_p below the ratios previously considered may ultimately result in the elimination of the hydraulic threshold and the disappearance of the well-mixed below-threshold condition.

Stovin *et al.* (2008 and 2010) have demonstrated that it is feasible to utilize validated CFD models to explore the flow field and solute transport regime for this type of system. This paper will therefore utilize a validated CFD modelling methodology to explore the mixing characteristics of small-diameter surcharged manholes. Findings will also be related to previous investigations into the systems' energy loss characteristics.

Methodology

CFD modelling methodology development and validation

Although it is now widely accepted that CFD has an important role to play in understanding complex flow fields and solute and sediment transport processes (see e.g. Jarman *et al*., 2008), the requirement to demonstrate that the models developed are robust and fit for specific purposes remains.

In the present paper, the CFD modelling methodology was developed and validated with reference to two complementary data sets: Guymer *et al.*, (2005) and Lau (2008). The Lau (2008) study primarily focused on scale effects, and replicated the 800 mm manhole experiments in a smaller-scale laboratory model (Φ_m = 218 mm, Φ_p = 24 mm, Φ_m/Φ_p = 9.1). As part of this study, high-resolution Particle Image Velocimetry (PIV) data was collected on both horizontal and vertical planes through the manhole for two specific conditions, s = 30 mm (0.138 Φ_m) and s = 80 mm (0.367 Φ_m). These correspond to below- and above-threshold conditions respectively, and solute trace data is also available for these specific conditions. The flowrate was 0.35 L/s.

The CFD modelling was undertaken in ANSYS Fluent versions 6 and 12. All geometry and mesh generation used GAMBIT. The CFD set-up is summarised in Table 1. The configuration options listed here were guided by previous studies (Lau, 2008; Stovin *et al.*, 2008), and by a number of specific parametric studies and grid-independence tests, the full details of which may be found in Bennett (2012) and Bennett *et al.* (2011). These studies included a detailed comparison of three alternative turbulence models (RSM, k-ε RNG and k-ε Realizable), a comparison between structured and unstructured mesh generation options, an investigation into whether the VOF (Volume-of-Fluid multiphase model) would improve the quality of the flow field, and comparisons between options for solute transport modelling (species model versus discrete phase model). The ultimate selection of options was guided primarily by model quality (as assessed using the validation procedures described below), although consideration was also given to ease of mesh generation, convergence speed and simulation stability.

The simulations used an unstructured tetrahedral mesh, with a meshing interval equivalent to $\Phi_p/8$ (3 mm in the 218 mm diameter manhole). The inlet boundary was modelled as a velocity inlet, with the velocity profile taken from the outlet of an independent simulation of a pipe of the same diameter. The outlet was represented using a pressure-outlet, and the free surface used a fixed-lid (zero friction) wall boundary. The walls were modelled using a roughness of 4 x 10^{-5} m (previously determined for laboratory perspex). The k–ε Realizable turbulence model was used, combined with non-equilibrium wall functions. Checks were undertaken to ensure that y^+ values were within a suitable range ($30 < y^+ < 300$). Solute transport was modelled using uncoupled particle tracking, with a discrete random walk model to represent the stochastic effects of turbulence. Each trace experiment was represented by more than 45,000 particles with density 998.2 kg/m^3 (as per water) and diameter 1×10^{-6} m. Particles were injected uniformly over the inlet surface, with the maximum number of steps set to 1×10^9 and the Time Scale Constant = 0.10. RTDs for the manhole system were generated from particle travel times monitored at the model outlet.

The CFD models were subjected to three levels of validation. Primary validation involved the qualitative comparison of the velocity fields on selected planes against Lau's (2008) PIV data. Two CFD models were developed, corresponding to the 218 mm manhole with s = 30 mm and s = 80 mm.

Secondary validation involved qualitative and quantitative comparisons of solute transport predictions against Lau's (2008) data. The RTDs were convolved with measured laboratory upstream temporal concentration profiles to synthesise downstream temporal concentration profile predictions. The R_t^2 parameter (Equation 1, Young *et al.*, 1980) was used to provide a measure of the goodness of fit of the predicted downstream temporal concentration profile to the measured data at the downstream site.

$$R_t^2 = 1 - \left[\frac{\sum_{t=1}^{n} \left(c(x_2, t) - p(x_2, t) \right)^2}{\sum_{t=1}^{n} \left(c(x_2, t) \right)^2} \right] \qquad \text{Equation 1}$$

The particle tracking results are directly interpretable as the system's RTD, i.e. the system's fundamental response to an instantaneous injection at its upstream end. Given that the system under consideration included both the manhole and its upstream and downstream pipe sections, the manhole RTD was determined by subtracting pipe travel times (assuming plug flow) from the total travel times. To enable manhole travel times to be compared independently of scale and specific flowrate, these travel times were normalised according to the manhole's nominal travel time ($t_n = V/Q$, where V represents manhole volume). The CRTD represents the Cumulative RTD, and t_{50} represents the median travel time.

The third level of validation focused specifically on a comparison of CRTDs and t_{50} values obtained following deconvolution of the original Guymer *et al.* (2005) laboratory data. The deconvolution process, together with a full analysis of the CRTDs corresponding to the 800 mm manhole, was detailed in Guymer and Stovin (2011). New CRTD data, corresponding to the three smaller diameter manholes will be presented here for the first time.

Identification of the threshold in small-diameter manholes

The validated CFD modelling methodology was utilised to replicate and extend the range of Φ_m/Φ_p ratios considered by Guymer *et al.* (2005) (Φ_p = 88 mm), and in particular to explore whether the hydraulic threshold (and its associated sudden change in mixing characteristics) would persist in the smaller diameter manholes more regularly encountered in practice. In addition to the four previously-considered configurations (Φ_m/Φ_p = 9.1, 6.8, 5.5 and 4.4), manholes with diameters 308, 220, 176 and 132 mm (Φ_m/Φ_p = 3.5, 2.5, 2.0 and 1.5) were also modelled. Each was modelled at a minimum of 9 different surcharge depths (s = 10 to 272 mm), with additional depths included where required to define the threshold level more accurately. 87 different combinations of manhole diameter and surcharge level were considered in total. As it has previously been shown that the threshold level is independent of flowrate, all simulations were undertaken at 1 l/s. However, for the largest manhole, additional simulations at 4 l/s were included to confirm this.

Identification of the presence or absence of the threshold surcharge level involved the visual inspection of flow fields and normalised CRTDs and an assessment of normalised t_{50} travel times plotted against surcharge level.

Results

CFD modelling methodology development and validation

Flow fields

Fig. 1 compares the simulated flow field (right-hand column) with the laboratory PIV flow field data (left-hand column) collected by Lau (2008) for a 218 mm diameter manhole (Φ_p = 24 mm). The data is presented for two validation cases: below-threshold (s = 30 mm) and above-threshold (s = 80 mm). Qualitatively it may be seen that the simulations effectively replicate the two contrasting flow regimes, the asymmetric below-threshold condition characterised by full mixing in the vertical plane, and the more-symmetric high surcharge condition characterised by short-circuiting. There are minor discrepancies, most notably surrounding the jet. In the low-surcharge case the jet core appears to extend too far into the manhole in the CFD simulation (see Fig. 1b), whereas in the high-surcharge case the jet core is a little weaker in the CFD simulation (Fig. 1f) than was observed in practice (Fig. 1e).

Solute traces

Figs. 2a and 2b compare the CFD-derived CRTDs with their laboratory counterparts for the two flow regimes. In this case the CRTDs are for the complete system, including the pipe sections upstream and downstream of the manhole. In Figs. 2c and 2d the CFD-derived RTDs have been convolved with the measured upstream temporal concentration profiles to generate downstream profiles that are directly comparable with the laboratory data. Figs. 2a and 2c include output from larger and smaller mesh densities than that used for the bulk of the simulations; they confirm that the chosen density was essentially grid-independent for the purposes of this study.

It may be seen that there is good agreement between the simulated solute transport characteristics and those observed in the laboratory. R_t^2 values for the simulated traces shown in Figs. 2c (3 mm mesh) and 2d are 0.983 and 0.994 respectively.

Threshold identification

The third level of validation focused on comparisons of the CFD results (CRTDs and t_{50} travel times) with the original Guymer *et al*. (2005) laboratory data for manholes with Φ_p = 88 mm and Φ_m of 800, 600, 485 and 385 mm. The deconvolution process used to derive CTRDs from the laboratory trace data has been described elsewhere (Guymer and Stovin, 2011), although data from the two smallest manholes has not been presented previously. It is important to note that there are some limitations to the laboratory data set (concerns about mass balance, incomplete mixing, incomplete/unrepresentative sampling of dye traces over the pipe cross-section, calibration errors, etc). Nonetheless, confirmation that the CFD model is able to replicate key trends observed in the laboratory over a range of higher Φ_m/Φ_p ratios provides confidence in its application to explore the processes acting in smaller diameter manholes.

Fig. 3a presents normalised CRTDs for the 800 mm laboratory manhole. This figure clearly shows the characteristic steep rise associated with short-circuiting effects in the high surcharge conditions. There is a very clear change from the highest below-threshold surcharge level (210 mm, s/Φ_m = 0.263) to the lowest above-threshold surcharge level (238 mm, s/Φ_m = 0.298). The below-threshold CRTDs do not collapse onto a single curve, as has previously been suggested. Instead, systematic variations are observed with mixing becoming increasingly well-developed as surcharge level increases. Particularly in the above-threshold cases, it may be seen that full mass recovery on the CRTDs was not observed, likely as a result of premature truncation of the tail of the downstream trace.

Fig. 3b presents the modelled data for the same configuration, and confirms that similar trends are reproduced. The sharp transition between the two hydraulic regimes appears to occur at a similar surcharge level (in this case $0.20 < s/\Phi_m < 0.27$). The same trends in the below-threshold CRTDs are apparent, although the systematic variation in below-threshold CRTDs appears to be greater in the CFD data than was observed in the laboratory data.

Figs. 3a and 3b suggest that the t_{50} parameter may be used as an indicator of the systematic variations in hydraulic regime as a function of surcharge. t_{50} values increase with surcharge up to the threshold level, s', and fall to a low, constant, value for surcharge levels > s'.

In Figs. 3c and 3d the variations in t_{50} values as a function of surcharge level for all four manhole diameters are compared. Both the laboratory and the modelled data sets provide strong indications of the existence of the hydraulic threshold (i.e. a sharp drop in t_{50} values at the threshold surcharge level), and both show that mixing effects increase approximately linearly with surcharge in the below-threshold region. The laboratory data appears to suggest that the threshold is spread over a range of levels ($0.2 < s/\Phi_m < 0.258$), whereas the CFD data suggests a sharper transition at close to $s/\Phi_m = 0.2$.

The laboratory data also supports the suggestions in the CFD data that, as the manhole diameter reduces, the maximum value of the normalised t_{50} decreases and the s/Φ_m ratio associated with the threshold appears to reduce. The CFD data appears to overestimate mixing in the high below-threshold region. This may be due to laboratory cut-off techniques; discrete-phase particle tracking ensures 100% mass recovery whereas this was not consistently achieved in the laboratory data.

Both laboratory and CFD data sets show that the normalised t_{50} in the above-threshold region increases as manhole diameter reduces. This is to be expected, as the short-circuiting jet flow bypasses a greater volume of inactive flow in the larger diameter manholes than in the smaller ones.

Validation Summary

Overall the validation process has demonstrated that the CFD modelling methodology is fit for purpose. The simulated flow fields capture key elements of these complex, jet-driven, confined, flows in two contrasting hydraulic regimes. The particle tracking model is capable of replicating observed downstream temporal concentration profiles with a high degree of accuracy. Lastly, it has been demonstrated that CFD-derived t_{50} values are consistent with those generated in the laboratory, and that they provide a robust indication of hydraulic regime that can be used with confidence to explore the existence of the hydraulic threshold in small-diameter manholes.

Identification of the threshold in small-diameter manholes

Flow fields

The left-hand column of Fig. 4 shows the simulated flow field on the central horizontal plane in four out of the eight simulated manholes, for flows with a surcharge level of 0.13 Φ_m. Note that the actual manhole diameter decreases from top to bottom; the pipe size is constant. The flow fields shown correspond to surcharge levels which are 'expected' to be below the hydraulic threshold, s'. Figs. 4a (Φ_m = 800 mm) and 4c (Φ_m = 600 mm) clearly show the asymmetric flow field associated with the below-threshold low-surcharge flow regime. The 308 mm diameter manhole (Fig. 4e) shows a slight deviation of the jet. However, in contrast to the larger diameter manholes, the high velocity core passes directly to the manhole outlet. The smaller diameter manholes (for example, the 220 mm manhole shown in Fig. 4g) show no obvious signs of the asymmetric jet. This suggests that, at Φ_m/Φ_p ratios below 3.5, the jet is fully restrained by the geometry of the manhole, and the highly-asymmetric (well mixed) below-threshold flow regime cannot be established. The flow field is more comparable with that observed in high-surcharge conditions (above-threshold) in larger-diameter manholes.

CRTDs

The normalised CRTDs for the full range of surcharge levels are presented for these same configurations in the right-hand column of Fig. 4. The 800 mm manhole CRTDs presented in Fig. 4b show clear groupings corresponding to the previously-identified flow regimes. At surcharge levels above the threshold, the CRTDs collapse onto a single curve. However, below the threshold a systematic variation in CRTD shape is observed, with the short-circuiting indicated by the steep initial rise in the CRTD increasing as surcharge decreases. The smallest amount of short-circuiting is evident when the surcharge level is just below the threshold. This is indicative of increased mixing within the manhole due to the highly asymmetric jet. Replicating data presented in Fig. 4b, Fig. 5 confirms that the normalised CRTDs are independent of flowrate.

At very low surcharges (10-20 mm), which have not been investigated in previous studies, a third grouping is present. Its characteristic CRTD shape is similar to that of the above-threshold condition.

The 600 mm manhole CRTDs (Fig. 4d) show similar behaviour to the 800 mm manhole data. There is a sharp discontinuity (i.e. the threshold) between the CRTDs corresponding to s/Φ_m = 0.18 and s/Φ_m = 0.20, and the below-threshold CRTDs show a systematic decrease in short-circuiting with increased surcharge.

In contrast, the CRTDs corresponding to the 308 and 220 mm manholes do not show any evidence of below-threshold, well-mixed, hydraulic regimes. Both the flow field plots and the CRTDs suggest that, at Φ_m/Φ_p ratios of 3.5 and below, the well-mixed, below-threshold flow regime is not established; instead the flow field is characterised by short-circuiting throughout the full range of surcharge levels. The gradient of the CRTDs is less steep in the larger manholes; this reflects the reduction in inactive manhole volume as Φ_m/Φ_p decreases.

Normalised t_{50} travel times

Fig. 6a shows normalised t_{50} against s/Φ_m. The 800 (Q = 1 and 4 l/s), 600, 485 and 385 mm manholes all exhibit a sharp step in normalised t_{50} travel times, confirming the existence of the hydraulic threshold. The 308 and 220 mm manholes do not exhibit a large step in t_{50} times, indicating the lack of an hydraulic threshold. Fig. 6a shows that for the manholes that do exhibit a hydraulic threshold, the region below-threshold is transitional in nature.

In Fig. 6b, the Y-axis scale has been normalised according to the equivalent travel time assuming the manhole was replaced by a pipe of the same length. The above-threshold conditions induce mixing equivalent to a pipe. In the below-threshold regime, as the manhole volume available for mixing decreases (Φ_m/Φ_p decreases), the normalised t_{50} values tend towards those expected for a pipe (i.e. plug flow).

Results for two different flowrates (Q = 1 l/s; Q = 4 l/s) are shown for the 800 mm manhole in Figs. 6a and 6b. These are nearly identical for all surcharge levels, confirming that the threshold location is independent of flow rate.

It has been hypothesised that a link exists between the Albertson *et al.* (1950) 1:5 jet expansion gradient and the ratio of the manhole diameter to the threshold level. This value (i.e. s' = 0.2 Φ_m) is indicated in Figs. 6a and 6b. The manholes with a Φ_m/Φ_p ratio greater than 5 (485, 600 and 800 mm diameter manholes) show an hydraulic threshold close to that of the Albertson *et al.* (1950) jet expansion limit. Below this limit, the 385 mm manhole (Φ_m/Φ_p = 4.4) also shows a step, indicative of a change in hydraulic regime. However, as the Φ_m/Φ_p ratio decreases, the surcharge required to cause a change in hydraulic regime also decreases. This deviation away from the idealised model may reflect the increasingly significant effects of confinement as the manhole diameter decreases.

Discussion

Variation in CRTD shape in the below-threshold region in large-diameter manholes

Guymer and Stovin (2011) identified consistent, systematic variations in CRTD shape in the below-threshold region. As with the current CFD-derived data, mixing appeared to increase (less steep CRTD) with increasing surcharge. The effects were less marked than the current data set, leading to the conclusion that the below-threshold region could be reasonably approximated using a single normalised CRTD. The current data set suggests, however, that an improved model of mixing for large-diameter, low-surcharge manholes should probably aim to account for these systematic variations.

Variations occur because the free surface places a vertical constraint on the jet expansion. As the surcharge level increases, the jet has more freedom to expand vertically, which also leads to enhanced transverse mixing, and more complete, chaotic mixing throughout the full manhole volume.

Comparison with the threshold surcharge level proposed by Guymer *et al.* (2005)

For manholes with $\Phi_m/\Phi_p \geq 4.4$, it has been shown that the threshold surcharge level, s', corresponds to 0.2 Φ_m. It has also been shown that this ratio is consistent with the theoretical model of jet expansion proposed by Albertson *et al.* (1950). However, the data originally presented by Guymer *et al.*, 2005, corresponded to s' = 0.258 Φ_m. There are certain limitations to the Guymer *et al.* (2005) data. The data was analysed using fitted ADE and ADZ models, which did not fit the measured data particularly well in many cases. The authors acknowledged scatter in their data set and qualified their findings with the suggestion that there may be a transition region rather than a distinct threshold. Equally, the discrepancies may reflect minor deficiencies in the CFD model's representation of the system, particularly the fixed lid free surface approximation and/or the turbulence model.

Conditions required to establish a well-mixed hydraulic regime in a surcharged manhole

Fig. 7 provides a schematic representation of the hydraulic conditions that occur in circular, un-benched, straight-through, surcharged manholes. Manhole A represents a system with $\Phi_m/\Phi_p \geq 4.4$, such as those considered in the previous (Guymer *et al.*, 2005) study; Manhole B is representative of the smaller-diameter manholes that have been considered for the first time in the present study. Flow patterns are characterised by short-circuiting unless two conditions apply, $\Phi_m/\Phi_p \geq 4.4$ and $s < \Phi_m/5$. This zone is highlighted with diagonal hatched shading in Fig. 7.

These two constraints are discussed below:

Manhole diameter constraint: $\Phi_m/\Phi_p \geq 4.4$ – The manhole diameter must be sufficiently large such that the incoming jet core can fully dissipate before it reaches the manhole outlet. For small diameter manholes (e.g. Manhole B), the jet tends to bridge the distance across the manhole, and minimal mixing (horizontal or vertical) is observed. In the present study, manholes with Φ_m of 308 mm and below ($\Phi_m/\Phi_p \leq 3.5$) showed no evidence of well-mixed behaviour at any surcharge levels, whereas manholes with Φ_m of 385 mm and above ($\Phi_m/\Phi_p \geq 4.4$) did exhibit the two distinct hydraulic regimes previously reported. Given the weakness of the threshold effects observed in the 385 mm manhole, $\Phi_m/\Phi_p = 4.4$ is taken as the lower limit for the development of well-mixed conditions below a threshold surcharge level.

Albertson *et al.* (1950) showed that for a free jet, the core velocity is retained for a distance of 6.2 Φ_p, irrespective of pipe velocity. For Φ_p = 88 mm, this suggests that the core velocity would not be present at the outlet for manholes with $\Phi_m \geq 550$ mm. However, the persistence of well-mixed conditions in the region ($4.4 < \Phi_m/\Phi_p < 6.2$) suggests either that the tip of the jet needs to penetrate some distance into the outlet pipe to induce short-circuiting effects, or that the geometrical constraints imposed by the manhole cause the jet to dissipate over a shorter distance than it would within an idealised semi-infinite volume.

Surcharge depth constraint: $s < \Phi_m/5$ – For manholes with $\Phi_m/\Phi_p \geq 4.4$ (e.g. Manhole A), the surcharge level must also be sufficiently shallow to enable the dissipating jet to promote mixing throughout the manhole's entire surcharge depth. It is evident that when s is high, the head of water in the overlying surcharge volume will tend to dampen the mixing effects associated with the diffusing jet, and that the characteristic above-threshold short-circuiting flows will develop. On the other hand, as s reduces, a critical depth will be reached at which the momentum associated with the diffusing jet as it impacts upon the manhole's downstream face will be sufficient to promote full mixing throughout the entire surcharge depth. Our observations suggest that the threshold level (s') is approximately equal to $\Phi_m/5$, consistent with the Albertson *et al.* (1950) theoretical model of jet expansion at 1:5.

Links between mixing and energy loss characteristics

Given that the transition between below-threshold well-mixed conditions and above-threshold short-circuiting conditions in large diameter manholes results from a fundamental change in the system's hydraulic regime, comparable changes in energy loss characteristics should also be evident. The energy loss owing to the manhole, ΔH, is defined as the difference in pressure head between the extrapolated upstream and downstream hydraulic grade lines at the manhole axis:

$$\Delta H = K\frac{u^2}{2g} \qquad \text{Equation 2}$$

where *K* is the energy loss coefficient, *u* is mean pipe velocity and *g* is gravitational acceleration.

Data presented by Lau *et al.* (2008) for laboratory manholes with $\Phi_m/\Phi_p = 9.1$ showed strong evidence of the links between flow regime, energy loss and solute transport, with *K* values falling sharply from near-constant values of approximately 1.0 below-threshold to around 0.45 for above-threshold surcharge depths. Energy loss data presented by Arao and Kusuda (1999) ($\Phi_m/\Phi_p = 3.6$) showed similar trends. High *K* values are associated with higher levels of energy dissipation in well-mixed flows; low *K* values reflect the reduced levels of energy dissipation associated with short-circuiting flow patterns.

The present study has introduced manholes with smaller Φ_m/Φ_p ratios than either of these studies. Fig. 6c presents *K* values for the current data set, calculated from the CFD pressure data. Consistent with the solute transport data (Fig. 6a) and with the previous studies, the data for the four largest manholes shows clear evidence of an hydraulic threshold. Also consistent with the solute transport data, the energy loss data suggests that the threshold does not arise in the two smaller diameter manholes, where short-circuiting tends to occur throughout the range of surcharge depths. The 308 mm manhole shows some evidence of transitional behaviour in both Figs. 6a and 6c. Its mixing and energy loss characteristics are similar to the larger manholes at low surcharge depths, but become more comparable with the 220 mm manhole at higher surcharge depths.

Implications for more complex manhole configurations

Both the normalised t_{50} and the energy loss coefficient *K* are dimensionless (scale-independent) parameters. The observations presented here are therefore applicable to full-scale systems (Lau *et al.,* 2008; Stovin *et al.*, 2010). However, it is recognised that the specific manhole configuration considered here is far simpler than many that are encountered in practice, which may include, for example, multiple inlets, angled outlets, benching or a drop in invert. Several of these configurations have been considered in previous laboratory studies, and selected findings will now be reviewed and interpreted with reference to jet theory and the underlying hydraulics.

In the unbenched manhole systems described earlier in this paper, well-mixed conditions were observed only when the incoming jet was unconfined and able to dissipate fully within the surcharge depth. It follows that the confining effects of benching will tend to prevent well-mixed conditions from ever developing and lead to short-circuiting flows throughout the range of surcharge depths. In contrast, the placement of the outlet at an angle from the inlet centreline will tend to enhance mixing. The impact of the jet on the downstream manhole wall is expected to lead to chaotic and well-mixed conditions at lower Φ_m/Φ_p ratios and/or at greater surcharge depths than with a straight-through outlet.

Saiyudthong (2003) investigated the effects of varying outlet angle in benched and unbenched surcharged manholes on solute transport and head loss, using a laboratory system with Φ_p = 88 mm and Φ_m = 388 mm. The outlet angles were 0° (i.e. straight-through), 30°, 60°, and 90° and flow rates were 1 l/s, 2 l/s, 4 l/s, 6 l/s and 8 l/s. Interestingly, with Φ_m/Φ_p = 4.4, this study lies just at the boundary of the conditions required for the hydraulic threshold that have been proposed here. Mixing characteristics were reported in terms of fitted ADE model mean travel times, and it should be noted that this approach has subsequently been shown to poorly represent this type of system, and may lead to significant loss of discrimination (Stovin *et al.*, 2010). The data suggests that at an outlet angle of 0°, the system behaved as a 'small diameter' manhole, i.e. there was little or no evidence of well-mixed flow conditions. However, the travel time data shows some evidence of the threshold (i.e. enhanced mixing at low levels of s) for outlet angles of 30° and 60° in unbenched manholes. With benching, there was no evidence of the threshold, or of well-mixed flow conditions, over the full range of outlet angles.

Sonnenwald *et al.* (2011) used deconvolution to recover CRTDs from a portion of Saiyudthong's original laboratory data (1 l/s, unbenched). Their analysis confirmed that whilst well-mixed conditions seemed not to occur at any surcharge depths for the 0° outlet angle configuration, they were increasingly evident as the outlet angle increased. The data also suggested that, as outlet angle increased, the threshold surcharge depth increased. For an outlet angle of 90°, the threshold surcharge depth approaches Φ_m, compared with approximately 0.2 Φ_m for a straight-through configuration.

The cases above provide qualitative support to hypotheses derived from an understanding of the system's fundamental hydraulics. Benching will tend to confine the jet, resulting in reduced mixing and minimal energy losses, whilst an angled outlet will tend to increase mixing and energy losses.

For more complex systems, even a descriptive assessment becomes problematic. Manholes are characterised by complex, interacting, hydrodynamic processes. Considerable research effort continues to be invested in empirical laboratory studies aimed at quantifying and modelling the integrated effects of a wide range of configuration variables. For example, Arao *et al*. (2011) build upon extensive previous laboratory-based experience to focus on drop manholes subjected to two inflows and four alternative inflow/outflow diameter and elevation combinations. The derived relationships for *K* incorporate seven separate non-dimensional parameters, one of which relates manhole diameter to the downstream pipe diameter. The current findings complement this work in three respects: firstly, it has been shown that significant thresholds exist in both the Φ_m/Φ_p ratio and s/Φ_m. It does not appear that these critical thresholds have been accounted for in any existing empirical relationships; secondly, we have shown that these relationships are linked to the inlet jet, which suggests that a dimensionless group based on inlet, rather than outlet, pipe diameter may prove to be more robust; and thirdly, CFD-based modelling tools have been shown to provide an effective alternative to physical laboratory tests. Given the infinite range of possible manhole configurations, it may be impractical to generate empirical relationships to accurately capture all possibilities. In complex cases, where accurate understanding is critical, specific studies will always be required. As computing power improves, it becomes feasible to anticipate the use of hybrid 1D/3D sewer network models that utilise simple hydraulics for the connecting pipes but expand out to 3D hydrodynamic CFD analysis for complex hydraulic structures at the nodes.

The similarities between Figs. 6a and 6c suggest that it might be feasible to use solute transport data to estimate energy losses, for example within real sewer systems. Alternatively, it should also be feasible to model a system's solute transport characteristics from known energy loss data. Further research into this aspect is recommended. Whilst the t_{50} parameter has been adopted here to characterise the hydraulic regime, there is likely to be value in considering a range of other parameters associated with the CRTD (Stovin *et al.,* 2008). For example, whilst t_{50} indicates the median residence time, t_{16} and t_{84} provide information about the system's dispersion characteristics.

Conclusions

A CFD modelling methodology has been developed to enable the flow fields and solute transport characteristics of small-diameter surcharged manholes ($\Phi_m/\Phi_p < 4.4$) to be studied. Validation comprised three stages: direct validation of flow fields against laboratory PIV measurements; indirect validation of CRTDs against laboratory solute trace tests; and the use of t_{50} values to identify the hydraulic threshold within a range of surcharge depths.

The hydraulic threshold previously identified for surcharged manholes is only evident in systems with large Φ_m/Φ_p ratios. In smaller-diameter manholes the incoming jet will tend to bridge the distance across the manhole such that short-circuiting effects dominate, irrespective of surcharge level. The critical Φ_m/Φ_p ratio has been found to be $\Phi_m/\Phi_p= 4.4$. Many manholes found in practice have Φ_m/Φ_p ratios of less than 4.4; their mixing characteristics can be assumed to be equivalent to a pipe.

In manholes with high Φ_m/Φ_p ratios, a low-surcharge, well-mixed, condition develops at surcharge levels below approximately 0.2 Φ_m. In contrast to previous findings, a systematic variation in CRTD shape has been observed, with the greatest mixing occurring at surcharge levels just below the hydraulic threshold.

Furthermore, at very low surcharges (10-20 mm), which have not been investigated in previous studies, a third hydraulic regime is present. Its characteristic CRTD shape is similar to that of the above-threshold condition.

Consistent with previous laboratory findings, data from the current CFD study has confirmed that the hydraulic threshold is also evident in the energy loss coefficients.

Acknowledgements

Paul Bennett was funded through an EPSRC Doctoral Training Account (DTA) scholarship.

References

Albertson, M. L., Dai, Y. B., Jensen, R. A., and Hunter, R. (1950). "Diffusion of submerged jets." *Trans. Am. Soc. Civ. Eng.*, 115, 639–664.

Arao, S., and Kusuda, T. (1999). "Effects of pipe bending angle on energy losses at two-way circular drop manholes." 8th Int. Conf. On Urban Storm Drainage, IWA, London, 2163–2168.

Arao, S., Kusuda, T., Moriyama, K., Hiratsuka, S.,Asada, J. and Hirose, N. (2011). "Energy loss at three-way circular drop manhole under surcharge flow", *12th Int. Conf. on Urban Drainage*, Porto Alegre, Brazil.

Bennett, P., Stovin, V. and Guymer, I. (2011). "Improved CFD simulation approaches for manhole mixing investigations", *12th Int. Conf. on Urban Drainage*, Porto Alegre, Brazil.

Bennett, P. (2012). "Evaluation of the solute transport characteristics of surcharged manholes using a RANS solution", Ph.D. thesis, Univ. of Sheffield, UK.

Camino, G.A., Zhu, D.Z. and Rajaratnam, N. (2012) "Jet Diffusion inside a confined chamber", J. Hydraulic Research, vol. 50, no. 1, 121-128.

Danckwerts, P.V. (1958). "Continuous flow systems". *Chemical Engineering Science*, Vol. 2, No. 1, 1-13.

Guymer, I., Dennis, P., O'Brien, R., and Saiyudthong, C. (2005). "Diameter and surcharge effects on solute transport across surcharged manholes." *J. Hydraul. Eng.*, 131(4), 312–321.

Guymer, I. and Stovin, V. R. (2011). "One Dimensional Mixing Model for Surcharged Manholes." *J. Hydraul. Eng. 137(10),* 1160-1172.

Jarman, D. S., Faram, M. G., Butler, D., Tabor, G., Stovin, V. R., Burt, D. and Throp, E., (2008) "Computational Fluid Dynamics as a tool for urban drainage system analysis: A review of applications and best practice", *11th Int. Conf. on Urban Drainage, 31 Aug - 5 Sept., Edinburgh, Scotland.*

Lau, S. D. (2008). "Scaling dispersion processes in surcharged manholes." Ph.D. thesis, Univ. of Sheffield, UK.

Lau, S., Stovin, V. R., and Guymer, I. (2008). “Scaling the solute transport characteristics of a surcharged manhole.” *Urban Water J*., 5(1), 33–42.

Levenspiel, O. (1972). Chemical reaction engineering, 2nd Ed., Wiley, New York.

Pedersen, F.B. and Mark, O. (1990) “Head losses in storm sewer manholes: submerged jet theory”, *J. Hydraulic Eng*., 116(11), 1317-1328.

Rajaratnam, N. (1976) Turbulent Jets. Amsterdam, Elsevier, Amsterdam NL.

Rajaratnam, N. and Subramanya, K. (1967) “Diffusion of rectangular wall jets in wider channels”, *J Hydraulic Research*, vol. 5, 281-294.

Saiyudthong, C. (2003). Effect of Changes in Pipe Direction across Surcharged Manholes on Dispersion and Head Loss. PhD thesis, University of Sheffield, England.

Sonnenwald, F., Stovin, V. and Guymer, I. (2011). “The influence of outlet angle on solute transport in surcharged manholes”, *12th Int. Conf. on Urban Drainage*, Porto Alegre, Brazil.

Stovin, V. R., Grimm, J. P., and Lau, S. D. (2008). “Solute transport modelling for urban drainage structures.” *J. Environ. Eng.*, 134(8), 640–650.

Stovin, V. R., Guymer, I., and Lau, S.-T. D. (2010). “Dimensionless method to characterize the mixing effects of surcharged manholes.” *J. Hydraul. Eng.*, 136(5), 318–327.

WRc. (2006). Sewers for Adoption – A Design and Construction Guide for Developers. Sixth Edition. Water Research Centre PLC.

Young, P., Jakeman, A. and McMurtie, R. (1980) “An instrument variable method for model order identification”, *Automatica,* 16, 281-294.

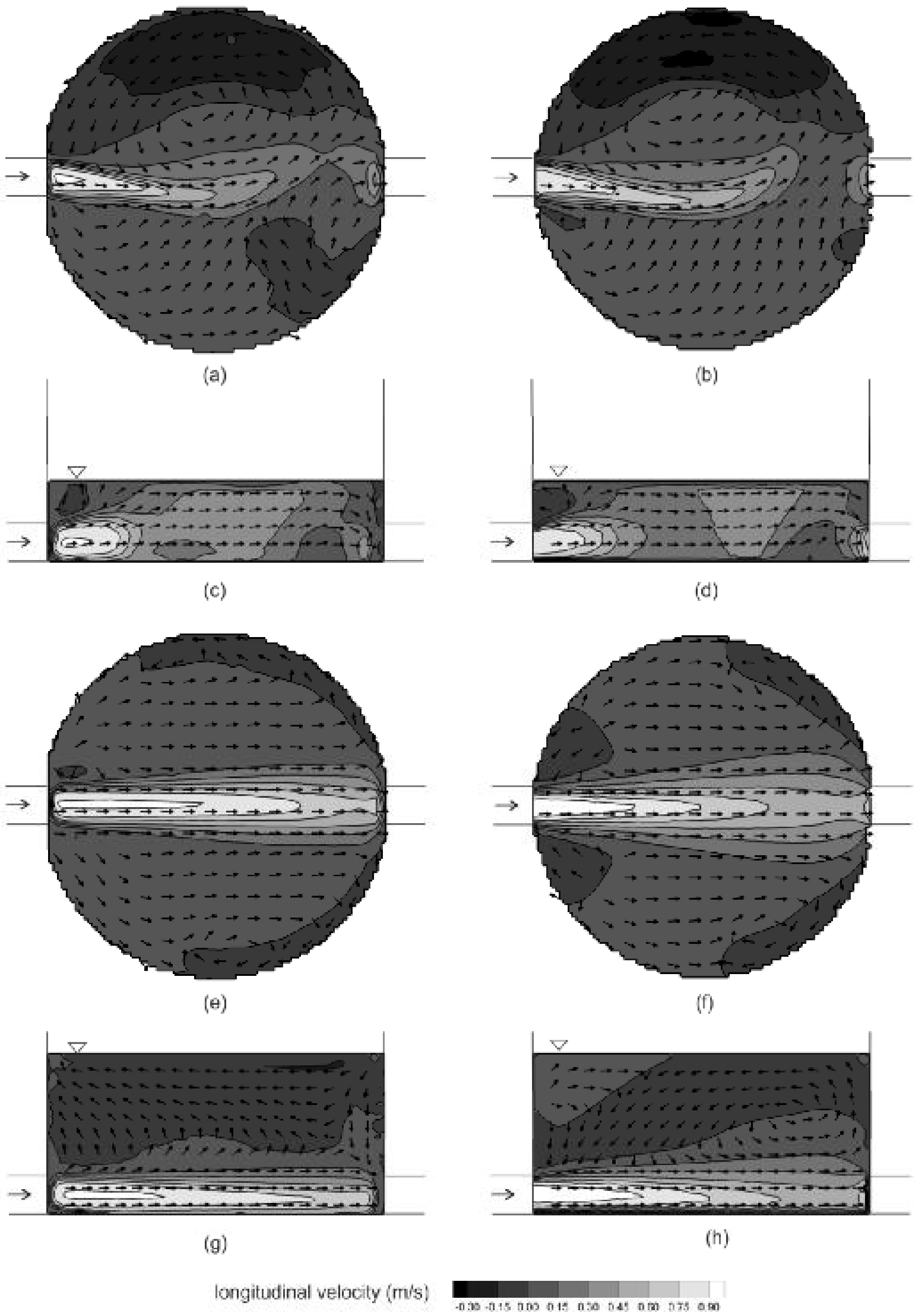

Figure 1 – Flow fields corresponding to the central horizontal plane (a, b, e and f) and the central vertical plane (c, d, g and h) for a 218 mm manhole (Q = 0.35 L/s) for PIV data (Lau (2008), left) and the CFD model (k-ε Realizable turbulence model, right). Contours are coloured by longitudinal velocity, vectors indicate flow direction. Plots (a) to (d) correspond to the below-threshold validation case, whereas plots (e) to (h) correspond to the above-threshold case.

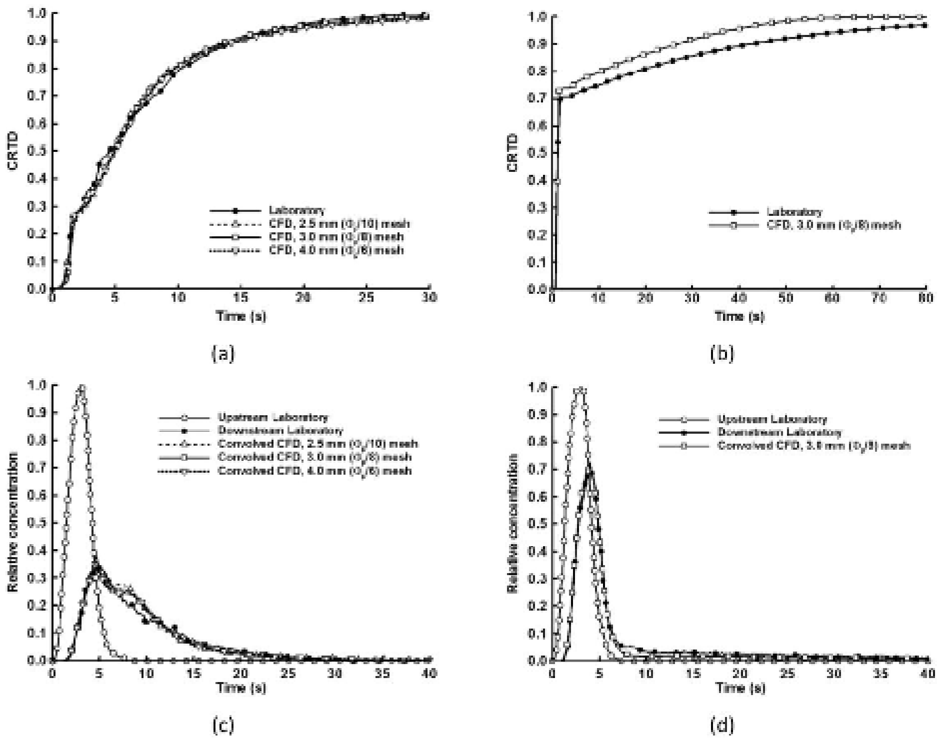

Figure 2 – CRTDs and downstream predictions compared with the laboratory results of Lau (2008). (a) and (b) show the CRTDs for below- and above-threshold conditions respectively. Laboratory CRTDs have been derived using deconvolution from laboratory trace data. (c) and (d) compare measured downstream concentration profiles with profiles synthesised by convolving the measured upstream trace with the CFD-derived CRTDs shown in (a) and (b).

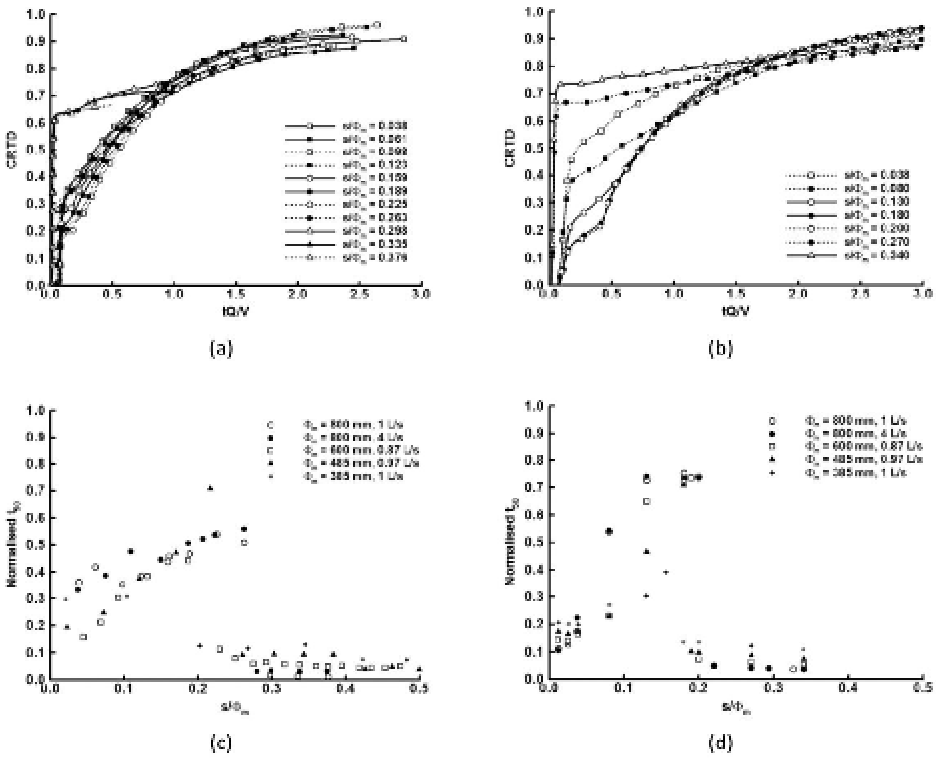

Figure 3 – Threshold identification. (a) and (c) present laboratory data (see Guymer *et al.*(2005) and Guymer and Stovin (2011)); (b) and (d) show the current CFD simulation results. (a) and (b) show CRTDs for the 800 mm diameter manhole with Q = 1 L/s; (c) and (d) show t_{50} travel times for the four different Φ_m/Φ_p ratios considered.

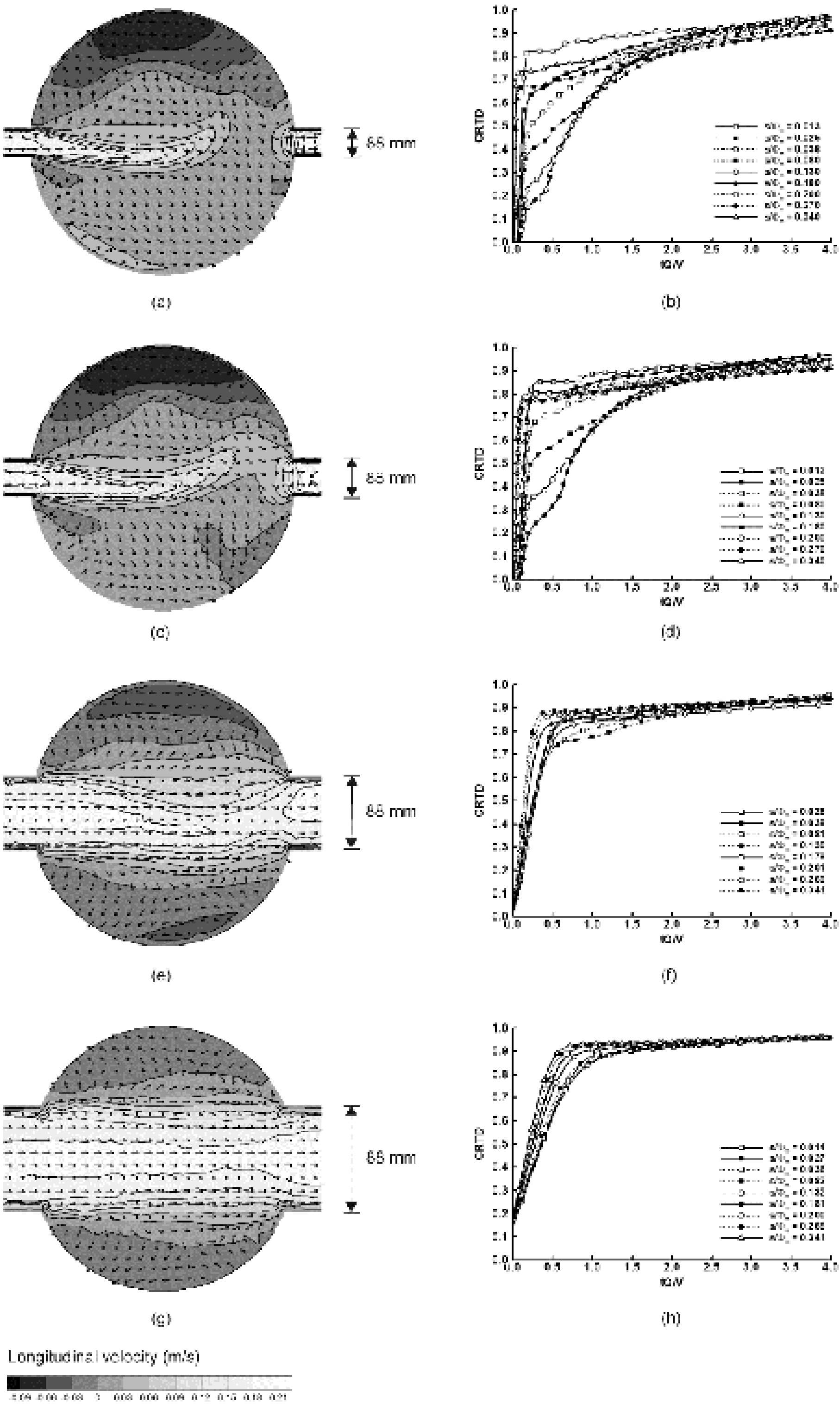

Figure 4 – Simulated flow fields (central horizontal plane, s = 0.13 Φ_m, left) and CRTDs for a range of manhole diameters and surcharge depths (right). In all cases Φ_p = 88 mm and Q = 1 L/s. (a) and (b) correspond to the 800 mm manhole (Φ_m/Φ_p = 9.1), (c) and (d) the 600 mm manhole Φ_m/Φ_p = 6.8), (e) and (f) the 308 mm manhole (Φ_m/Φ_p = 3.5) and (g) and (h) the 220 mm manhole (Φ_m/Φ_p = 2.5).

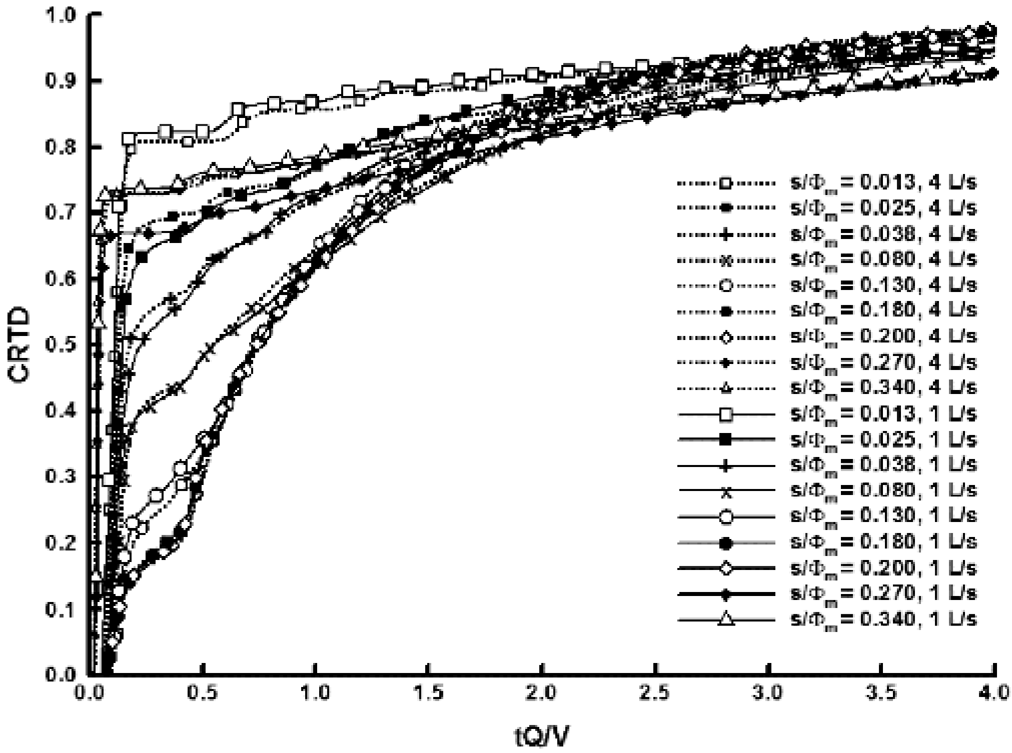

Figure 5 – The effect of flowrate on normalised CFD-derived CRTDs.

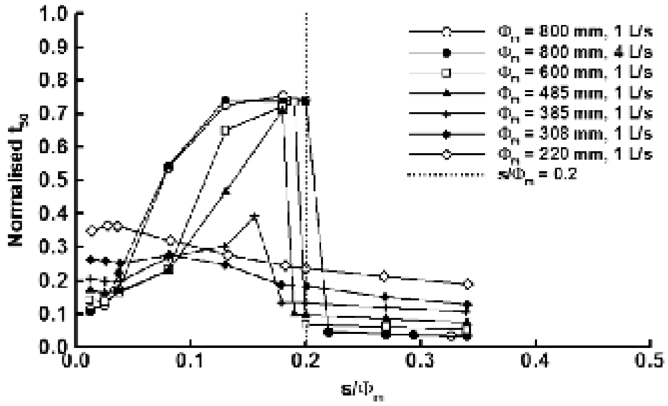

(a)

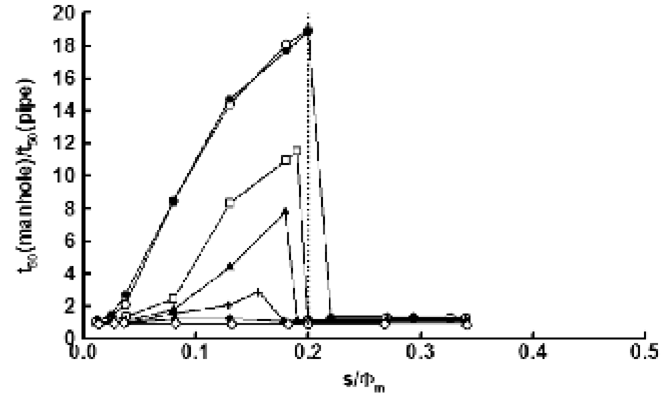

(b)

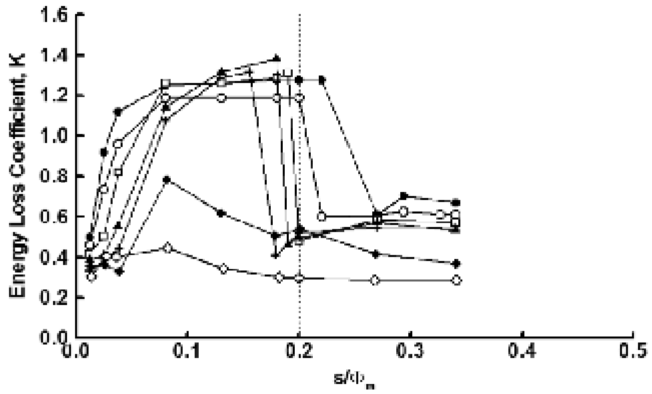

(c)

Figure 6 – Travel times and energy loss coefficients as a function of s/Φ_m. The dotted line indicates s/Φ_m = 0.2, which equates to the upper limit of the jet dissipation zone according to Albertson *et al*., (1950).
(a) Normalised t_{50} travel times; (b) t_{50} travel times normalised with respect to an equivalent pipe length; (c) Energy loss coefficient, *K*.

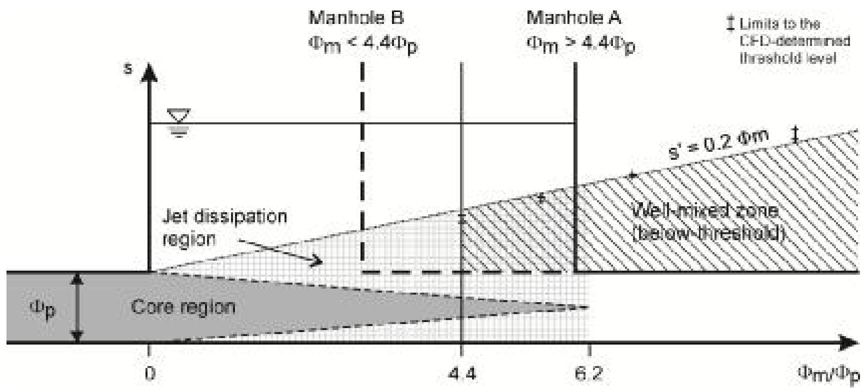

Figure 7 **–** Hydraulic conditions associated with well-mixed flow in surcharged circular manholes. Jet dissipation associated with an ideal discharge into a semi-infinite volume (after Albertson *et al.*, 1950) is also indicated.

Table 1 Validated set-up parameters for meshing, solving and modelling solute transport

Parameter	Setting/Value
Mesh:	
Meshing Strategy	Unstructured, fixed-lid
Face Mesh	Tri-pave
Volume Mesh	Tgrid
Reference Face	Inlet
Inlet boundary	Velocity-inlet
Outlet boundary	Pressure-outlet
Top boundary	Wall (zero friction)
Wall boundary	Wall (Perspex)
Mesh interval	3 mm (Φ_p/8)
y^+ values	$30 < y^+ < 300$
Solver:	
Pressure	PRESTO
Momentum terms	QUICK
Velocity-pressure coupling	SIMPLEC
Turbulence Model	k-ε Realizable
Gravity	Yes
Boundary wall roughness	0 m, 4×10^{-5} m
Near-wall treatment	Non-equilibrium wall functions
Residuals	1×10^{-5}
Solute:	
Model	Uncoupled particle tracking
Discrete random walk	Yes
No. of particles	>45,000
Particle density	998.2 kg/m^3 (as per water)
Particle size	1×10^{-6} (uniform)
Injection	from surface (inlet)
Max no. of steps	1×10^9 (maximum)
Time Scale Constant	0.10